10. Konstam MA, Neaton JD, Dickstein K, Drexler H, Komajda M, Martinez FA, Riegger GA, Malbecq W, Smith RD, Guptha S, Poole-Wilson PA. Effects of high-dose versus low-dose losartan on clinical outcomes in patients with heart failure (HEAAL study): a randomised, double-blind trial. *Lancet* 2009;**374**:1840–1848.
11. Radford MJ, Arnold JM, Bennett SJ, Cinquegrani MP, Cleland JG, Havranek EP, Heidenreich PA, Rutherford JD, Spertus JA, Stevenson LW, Goff DC, Grover FL, Malenka DJ, Peterson ED, Redberg RF. ACC/AHA key data elements and definitions for measuring the clinical management and outcomes of patients with chronic heart failure: a report of the American College of Cardiology/American Heart Association Task Force on Clinical Data Standards (Writing Committee to Develop Heart Failure Clinical Data Standards): developed in collaboration with the American College of Chest Physicians and the International Society for Heart and Lung Transplantation: endorsed by the Heart Failure Society of America. *Circulation* 2005;**112**:1888–1916.
12. Hall MJ, Levant S, DeFrances CJ. Hospitalization for congestive heart failure: United States. *NCHS Data Brief* 2000–2010;**2012**:1–8.
13. Mortara A, La Rovere MT, Pinna GD, Prpa A, Maestri R, Febo O, Pozzoli M, Opasich C, Tavazzi L. Arterial baroreflex modulation of heart rate in chronic heart failure: clinical and hemodynamic correlates and prognostic implications. *Circulation* 1997;**96**:3450–3458.
14. La Rovere MT, Bigger JT Jr, Marcus FI, Mortara A, Schwartz PJ. Baroreflex sensitivity and heart-rate variability in prediction of total cardiac mortality after myocardial infarction. ATRAMI (Autonomic Tone and Reflexes After Myocardial Infarction) Investigators. *Lancet* 1998;**351**:478–484.
15. Li M, Zheng C, Sato T, Kawada T, Sugimachi M, Sunagawa K. Vagal nerve stimulation markedly improves long-term survival after chronic heart failure in rats. *Circulation* 2004;**109**:120–124.
16. Li M, Zheng C, Inagaki M, Kawada T, Sunagawa K, Sugimachi M. Chronic vagal stimulation decreased vasopressin secretion and sodium ingestion in heart failure rats after myocardial infarction. *Conf Proc IEEE Eng Med Biol Soc* 2005;**4**:3962–3965.
17. De Ferrari GM, Crijns HJ, Borggrefe M, Milasinovic G, Smid J, Zabel M, Gavazzi A, Sanzo A, Dennert R, Kuschyk J, Raspopovic S, Klein H, Swedberg K, Schwartz PJ. Chronic vagus nerve stimulation: a new and promising therapeutic approach for chronic heart failure. *Eur Heart J* 2011;**32**:847–855.
18. Schwartz PJ. Vagal stimulation for heart diseases: from animals to men. An example of translational cardiology. *Neth Heart J* 2013;**21**:82–84.
19. Lazartigues E, Freslon JL, Tellioglu T, Brefel-Courbon C, Pelat M, Tran MA, Montastruc JL, Rascol O. Pressor and bradycardic effects of tacrine and other acetylcholinesterase inhibitors in the rat. *Eur J Pharmacol* 1998;**361**:61–71.
20. Androne AS, Hryniewicz K, Goldsmith R, Arwady A, Katz SD. Acetylcholinesterase inhibition with pyridostigmine improves heart rate recovery after maximal exercise in patients with chronic heart failure. *Heart* 2003;**89**:854–858.
21. Okazaki Y, Zheng C, Li M, Sugimachi M. Effect of the cholinesterase inhibitor donepezil on cardiac remodeling and autonomic balance in rats with heart failure. *J Physiol Sci* 2010;**60**:67–74.
22. Li M, Zheng C, Kawada T, Inagaki M, Uemura K, Shishido T, Sugimachi M. Donepezil markedly improves long-term survival in rats with chronic heart failure after extensive myocardial infarction. *Circ J* 2013;**77**:2519–2525.
23. Lefebvre F, Préfontaine A, Calderone A, Caron A, Jasmin JF, Villeneuve L, Dupuis J. Modification of the pulmonary renin-angiotensin system and lung structural remodelling in congestive heart failure. *Clin Sci (Lond)* 2006;**111**:217–224.
24. Kawada T, Li M, Kamiya A, Shimizu S, Uemura K, Yamamoto H, Sugimachi M. Open-loop dynamic and static characteristics of the carotid sinus baroreflex in rats with chronic heart failure after myocardial infarction. *J Physiol Sci* 2010;**60**:283–298.
25. Suga H. *Ventricular energetics. Physiol Rev* 1990;**70**:247–277.
26. Bristow MR. Treatment of chronic heart failure with β-adrenergic receptor antagonists: a convergence of receptor pharmacology and clinical cardiology. *Circ Res* 2011;**109**:1176–1194.
27. Swedberg K1, Komajda M, Böhm M, Borer JS, Ford I, Dubost-Brama A, Lerebours G, Tavazzi L, SHIFT Investigators, Ivabradine and outcomes in chronic heart failure (SHIFT): a randomised placebo-controlled study. *Lancet* 2010;**376**: 875–85.
28. Matsuura W, Sugimachi M, Kawada T, Sato T, Shishido T, Miyano H, Nakahara T, Ikeda Y, Alexander J Jr, Snagawa K. Vagal stimulation decreases left ventricular contractility mainly through negative chronotropic effect. *Am J Physiol* 1997;**273**:H534–H539.
29. Nakayama Y, Miyano H, Shishido T, Inagaki M, Kawada T, Sugimachi M, Sunagawa K. Heart rate-independent vagal effect on end-systolic elastance of the canine left ventricle under various levels of sympathetic tone. *Circulation* 2001;**104**:2277–2279.
30. Joaquim LF, Farah VM, Bernatova I, Fazan R Jr, Grubbs R, Morris M. Enhanced heart rate variability and baroreflex index after stress and cholinesterase inhibition in mice. *Am J Physiol Heart Circ Physiol* 2004;**287**:H251–H257.
31. Singer W, Opfer-Gehrking TL, Nickander KK, Hines SM, Low PA. Acetylcholinesterase inhibition in patients with orthostatic intolerance. *J Clin Neurophysiol* 2006;**23**:476–481.
32. Rosas-Ballina M, Tracey KJ. Cholinergic control of inflammation. *J Intern Med* 2009;**265**:663–679.
33. Mann DL. Inflammatory mediators and the failing heart: past, present, and the foreseeable future. *Circ Res* 2002;**91**:988–998.
34. Springer J, Okonko DO, Anker SD. Vagal nerve stimulation in chronic heart failure: an antiinflammatory intervention? *Circulation 2004*;**110**:e34; author reply e34.
35. Schellings MW, Pinto YM, Heymans S. Matricellular proteins in the heart: possible role during stress and remodeling. *Cardiovasc Res* 2004;**64**:24–31.
36. Ertl G, Frantz S. Healing after myocardial infarction. *Cardiovasc Res* 2005;**66**:22–32.
37. Heeschen C, Weis M, Aicher A, Dimmeler S, Cooke JP. A novel angiogenic pathway mediated by non-neuronal nicotinic acetylcholine receptors. *J Clin Invest* 2002;**110**:527–536.
38. Zheng W, Brown MD, Brock TA, Bjercke RJ, Tomanek RJ. Bradycardia-induced coronary angiogenesis is dependent on vascular endothelial growth factor. *Circ Res* 1999;**85**:192–198.
39. Milavetz JJ, Raya TE, Johnson CS, Morkin E, Goldman S. Survival after myocardial infarction in rats: captopril versus losartan. *J Am Coll Cardiol* 1996;**27**:714–719.
40. Cohn JN, Tognoni G, Valsartan Heart Failure Trial Investigators. A randomized trial of the angiotensin-receptor blocker valsartan in chronic heart failure. *N Engl J Med* 2001;**345**:1667–1675.
41. Richer C, Fornes P, Cazaubon C, Domergue V, Nisato D, Giudicelli JF. Effects of long-term angiotensin II AT1 receptor blockade on survival, hemodynamics and cardiac remodeling in chronic heart failure in rats. *Cardiovasc Res* 1999;**41**:100–108.
42. Takahashi M, Tanonaka K, Yoshida H, Oikawa R, Koshimizu M, Daicho T, Toyo-Oka T, Takeo S. Effects of ACE inhibitor and AT1 blocker on dystrophin-related proteins and calpain in failing heart. *Cardiovasc Res* 2005;**65**:356–365.
43. Urata H, Kinoshita A, Misono KS, Bumpus FM, Husain A. Identification of a highly specific chymase as the major angiotensin II-forming enzyme in the human heart. *J Biol Chem* 1990;**265**:22348–22357.
44. Lanctôt PM, Leclerc PC, Escher E, Leduc R, Guillemette G. Role of N-glycosylation in the expression and functional properties of human AT1 receptor. *Biochemistry* 1999;**38**:8621–8627.
45. Pfeffer MA, Pfeffer JM, Steinberg C, Finn P. Survival after an experimental myocardial infarction: beneficial effects of long-term therapy with captopril. *Circulation* 1985;**72**:406–412.
46. Ahmet I, Morrell C, Lakatta EG, Talan MI. Therapeutic efficacy of a combination of a beta1-adrenoreceptor (AR) blocker and beta2-AR agonist in a rat model of postmyocardial infarction dilated heart failure exceeds that of a beta1-AR blocker plus angiotensin-converting enzyme inhibitor. *J Pharmacol Exp Ther* 2009;**331**:178–185.
47. White HD, Aylward PE, Huang Z, Dalby AJ, Weaver WD, Barvik S, Marin-Neto JA, Murin J, Nordlander RO, van Gilst WH, Zannad F, McMurray JJ, Califf RM, Pfeffer MA. Mortality and morbidity remain high despite captopril and/or valsartan therapy in elderly patients with left ventricular systolic dysfunction, heart failure, or both after acute myocardial infarction: results from the Valsartan in Acute Myocardial Infarction Trial (VALIANT). *Circulation* 2005;**112**:3391–3399.
48. Nordström P, Religa D, Wimo A, Winblad B, Eriksdotter M. The use of cholinesterase inhibitors and the risk of myocardial infarction and death: a nationwide cohort study in subjects with Alzheimer's disease. *Eur Heart J* 2013;**34**:2585–2591.

Progress in Biophysics and Molecular Biology 115 (2014) 129–139

Contents lists available at ScienceDirect

Progress in Biophysics and Molecular Biology

journal homepage: www.elsevier.com/locate/pbiomolbio

Review

Relevance of cardiomyocyte mechano-electric coupling to stretch-induced arrhythmias: Optical voltage/calcium measurement in mechanically stimulated cells, tissues and organs

Kinya Seo [a], Masashi Inagaki [b], Ichiro Hidaka [c], Hana Fukano [d], Masaru Sugimachi [b], Toshiaki Hisada [d], Satoshi Nishimura [e, f], Seiryo Sugiura [d, *]

[a] Division of Cardiology, Department of Medicine, The Johns Hopkins Medical Institutions, Baltimore, MD 21205, USA
[b] Department of Cardiovascular Dynamics, National Cerebral and Cardiovascular Center Research Institute, Osaka 565-0873, Japan
[c] Division of Physical and Health Education, Graduate School of Education, The University of Tokyo, Tokyo 113-0033, Japan
[d] Department of Human and Engineered Environmental Studies, Graduate School of Frontier Sciences, The University of Tokyo, 5-1-5 Kashiwanoha, Kashiwa, Chiba 277-8563, Japan
[e] Research Division of Cell and Molecular Medicine, Center for Molecular Medicine, Jichi Medical University, Tochigi 329-0498, Japan
[f] Department of Cardiovascular Medicine, Translational Systems Biology and Medicine Initiative, The University of Tokyo, Tokyo 113-8655, Japan

ARTICLE INFO

Article history:
Available online 30 July 2014

Keywords:
Mechano-electric coupling
Stretch-induced arrhythmia
Commotio cordis
Carbon-fiber
Optical mapping
Optical trap

ABSTRACT

Stretch-induced arrhythmias are multi-scale phenomena in which alterations in channel activities and/or calcium handling lead to the organ level derangement of the heart rhythm. To understand how cellular mechano-electric coupling (MEC) leads to stretch-induced arrhythmias at the organ level, we developed stretching devices and optical voltage/calcium measurement techniques optimized to each cardiac level. This review introduces these experimental techniques of (1) optical voltage measurement coupled with a carbon-fiber technique for single isolated cardiomyocytes, (2) optical voltage mapping combined with motion tracking technique for myocardial tissue/whole heart preparations and (3) real-time calcium imaging coupled with a laser optical trap technique for cardiomyocytes. Following the overview of each methodology, results are presented. We conclude that individual MEC in cardiomyocytes can be heterogeneous at the ventricular level, especially when moderate amplitude mechanical stretches are applied to the heart, and that this heterogeneous MEC can evoke focal excitation that develops into re-entrant arrhythmias.

Contents

* Corresponding author. Tel.: +81 3 5841 8393; fax: +81 3 5841 6376.
E-mail addresses: seokin54@gmail.com (K. Seo), masashii@ncvc.go.jp (M. Inagaki), hidaka@p.u-tokyo.ac.jp (I. Hidaka), hanaff87@gmail.com (H. Fukano), su91mach@ncvc.go.jp (M. Sugimachi), hisada@mech.t.u-tokyo.ac.jp (T. Hisada), snishi-tky@umin.ac.jp (S. Nishimura), sugiura@k.u-tokyo.ac.jp (S. Sugiura).

http://dx.doi.org/10.1016/j.pbiomolbio.2014.07.008
0079-6107/

1. Introduction

Alterations in the mechanical state of the heart can affect its electrophysiological behavior (Kohl et al., 2011; Ravens, 2003; Taggart and Lab, 2008). This mechano-electric coupling (MEC) is considered to play an important role in cardiac rhythm abnormalities, especially in disease states such as old myocardial infarction and chronic heart failure, in which ventricular walls are subjected to abnormal hemodynamic loading stresses (Aimond et al., 1999; Janse, 2004; Tomaselli and Marban, 1999). Sudden mechanical impact to the heart can also disarrange the heart rhythm even in healthy subjects, which in some instances leads to sudden cardiac death (Link, 2012). However, this phenomenon (termed *commotio cordis*) is rare, and evidence linking mechanical impact to fatal arrhythmias is scarce.

The mechanisms underlying MEC relate to the activation of ion channels by mechanical stretch (Sachs, 2010, 2011). Because such stretch-activated channels (SACs) have long been suspected as important contributors to MEC, there are many reports on characterization of these channels (Bett and Sachs, 2000; Craelius et al., 1988; Kohl et al., 1998; Niu and Sachs, 2003; Ward et al., 2008). In particular, considering the physiological loading conditions for each myocyte in the ventricular wall, numerous studies have been performed in isolated cardiomyocytes in response to axial stretching to elucidate the properties of SACs (Belus and White, 2003; Iribe et al., 2010; Kamkin et al., 2003; Riemer and Tung, 2003; Sasaki et al., 1992; Zeng et al., 2000). However, single channel recording in the stretch-imposed ventricular myocytes demands technical proficiency because of the difficulty in maintaining stable attachment of the glass electrode during the stretch. These restrictions also impair the ability to study the dynamic properties of cellular MEC induced by transient mechanical stretches.

Recent studies have revealed that axial stretching of cardiomyocytes enhances Ca^{2+} spark/wave rate via mechanisms dependent on microtubule-mediated modulation (Iribe et al., 2009), NADPH2 oxidase (NOX2) activation (Prosser et al., 2011) and neuronal nitric oxide synthase (nNOS) activation (Jian et al., 2014) of the ryanodine receptor. On the one hand, stretch acutely increases the affinity of troponin C to Ca^{2+} (Allen and Kentish, 1988), so that when stretched tissue is released there is a surge in intracellular Ca^{2+}, which can lead to Ca^{2+} waves (ter Keurs et al., 2008). These spontaneous Ca^{2+} releases are regarded as an important substrate for triggered arrhythmias and delayed after depolarizations (Fujiwara et al., 2008), though whether SACs and/or Ca^{2+} cycling contributes to MEC-related arrhythmias is unclear.

To clarify how MEC contributes to ventricular arrhythmias, various studies have been performed with cardiac tissues and whole heart preparations (Fasciano and Tung, 1999; Franz et al., 1992; Hansen et al., 1990; Parker et al., 2001). However, many of these reports are limited owing to lack of experimental methodologies for recording the electrical and mechanical activity simultaneously and with high spatiotemporal resolution. For instance, optical mapping (Efimov et al., 2004; Herron et al., 2012), a technique used to examine spatiotemporal electrical behavior in the heart, often necessitates either physically or pharmacologically constraining the heart contraction, which limits its utility for MEC research.

Herein, we review our techniques that we developed to resolve these various methodological issues in isolated cardiac myocytes (Section 2) and myocardial tissues (Section 3). Next, we discuss a possible scenario for the link between cellular MEC and fatal arrhythmias (Section 4). Furthermore, we briefly introduce our ongoing studies using an optical trap technique to elucidate the mechanisms of stretch-mediated Ca^{2+} handling (Section 5), and then provide a final conclusion (Section 6).

2. Cardiomyocyte study

There are only a small number of studies reporting the characteristics of cardiomyocytes MEC upon axial stretching. Considering the dynamic changes in stress and strain that an individual cardiomyocyte experiences in the beating heart, it is important to examine the responses to dynamic stretching on single cardiomyocytes. In this section, we introduce our methodology for examining single cardiomyocytes, in which we combine a carbon-fiber technique with optical voltage measurement for assessing cellular MEC upon dynamic stretching.

2.1. Carbon-fiber technique for single cardiomyocyte stretching

Single adult cardiomyocytes have been widely used to relate subcellular molecular events to functional characteristics of the heart. The simple geometry of a myocyte offers substantial advantages over multicellular preparations due to the fairly homogeneous strain distribution and exogenous factors (Palmer et al., 1996; Yasuda et al., 2001). However, they are notoriously difficult to manipulate and maintain because of the irritability and fragility of the sarcolemma. A number of techniques have been proposed to overcome these limitations. For example, Kamkin applied local stretches to ventricular myocytes by pulling with a glass stylus and patch-pipette (Kamkin et al., 2000), while Zeng and Riemer used a pair of suction pipettes to pull the myocyte from each end (Riemer and Tung, 2003; Zeng et al., 2000). A totally different technique was introduced by Le Guennec (Le Guennec et al., 1990) in which a pair of thin carbon fibers was attached to the myocyte surface, likely because of electrostatic forces between the fibers and the surface (Garnier, 1994). This technique was later modified with the use of graphite-reinforced carbon (GRC; Tsukuba Material Information Laboratory Ltd, Tsukuba, Japan) fiber (Sugiura et al., 2006) and/or biocompatible adhesive (MyoTak; IonOptix, Milton, MA, USA; or World Precision Instruments Inc., Sarasota, FL, USA) (Khairallah et al., 2012; Prosser et al., 2011) to enable firmer attachment between the fibers and the cellular surface, and was used for the dynamic stretching of single cardiomyocytes (Nishimura et al., 2006a, 2006b; Seo et al., 2014).

We typically use a pair of carbon fibers and attach them to each end of a cardiomyocyte to clamp it under a microscope (Sugiura et al., 2006). One fiber is rigid to serve as a mechanical anchor, while the other fiber is compliant and controlled quickly and digitally by a connected piezoelectric transducer (P-841.40; Physik Instrumente, Karlsruhe, Germany). The magnitude of the bending motion of the compliant carbon fiber is monitored by a fast digital dimensioning CCD camera (IonOptix, Milton, MA, USA) (Fig. 1A) to calculate the contractile force by multiplying by the fiber stiffness. The attachment of the carbon fibers to the myocyte surface results

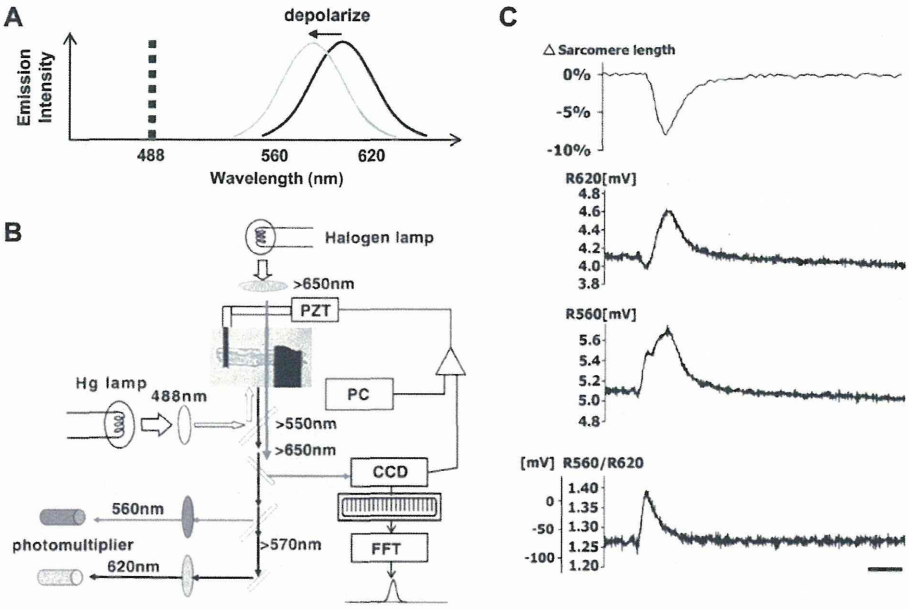

Fig. 1. A) Scheme of the fluorescence properties of di-8-ANEPPS. The dye was excited at 488 nm (dashed line) and two emission lights were detected separately in 560 and 620 nm wavelength bands (shaded boxes). B) Diagram of the experimental setup for cardiomyocyte study. A pair of carbon fibers was attached to the myocyte surface, and the thin fiber was controlled by a piezoelectric translator (PZT) connected to a personal computer (PC). The positions of the carbon fibers were captured by a charge-coupled device camera (CCD), and the sarcomere length was measured by fast Fourier transformation (FFT). For optical voltage measurement, the dye was excited at 488 nm, and the emission light was recorded ratiometrically by two photomultipliers (560 and 620 nm). A long wavelength (>650 nm) was used for the CCD observation. C) Ratiometry of cardiomyocyte action potential. During active contraction indicated by sarcomere shortening, red (620 nm) and green (560 nm) fluorescence signals (raw voltage signals) were recorded with two photomultipliers separately. Ratiometry (R560/R620) successfully removed the motion artifacts. Scale bars: 100 ms.

in minimal damage to the sarcolemma (Gannier et al., 1994) and reduces the need for technical proficiency. Importantly, this technique does not interfere with simultaneous recording of the sarcomere striation and the fluorescent membrane voltage measurement (Nishimura et al., 2006a, 2008) described below.

This carbon-fiber technique can be applied to various experiments with some modifications. For instance, the force–length relationship (Frank-Starling Mechanism) of a single cardiomyocyte can be assessed by measuring contractile force and sarcomere shortening at various stretch levels (Iribe et al., 2007; Nishimura et al., 2004; Scimia et al., 2012; White et al., 1993). Modified techniques were used for assessing slow force responses (Calaghan and White, 2004; Seo et al., 2014) and Ca^{2+} spark/wave rates (Iribe et al., 2009; Prosser et al., 2011) by combining the stretch apparatus with fluorescent calcium measurement. Furthermore, by attaching a latex microsphere to the side of the tip of the compliant carbon fiber, the indentation test can be applied by pushing it against the myocyte horizontally (Nishimura et al., 2006b). Shear strain can be also applied by shifting the glass flake connected to a piezoelectric translator via the carbon fiber in both the longitudinal and transverse plane (Nishimura et al., 2006b).

2.2. Fluorescent voltage measurement in single cardiomyocytes

The influence of mechanical stretch on the membrane potential is one of the major fields of MEC research. We coupled the carbon-fiber technique with fluorescent voltage measurement using a transmembrane voltage-sensitive dye, which allows us to avoid the motion contamination often detected in standard patch-pipette voltage recording. Voltage-sensitive dyes can be used to monitor fast events such as action potentials and membrane depolarization, and ratiometric evaluation of two simultaneously detected emission wavelengths can effectively remove motion artifacts often detected by the standard patch-pipette technique (Knisley et al., 2000; Tai et al., 2004). However, voltage-sensitive dyes have some weaknesses. First, because voltage-sensitive dyes only provide a measurement of relative voltage change, the fluorescent signal should be calibrated against the direct electrode measurement. Second, since phototoxicity of the dye to cardiomyocytes is not negligible under high-dose (30–60 μM), it should be prevented by limiting the loading dose of the dye, reducing the illumination wattage and adding a combination of antioxidants (catalase, glucose oxidase and Trolox C) (Bullen and Saggau, 1999; Schaffer et al., 1994). We used di-8-ANEPPS, a ratiometric dye, with its emission spectrum shifting reversibly to shorter wavelengths in response to membrane depolarization (Fig. 1A). The emitted light for shorter wavelengths (560 nm) increases simultaneously with the decrease in the emitted light for longer wavelength (620 nm) during depolarization. Hence, the ratiometry of these two wavelengths theoretically cancels out the changes in fluorescence intensity caused by motion. A diagram of our experimental system is shown in Fig. 1B. After excitation of the dye at 488 nm with a filtered mercury light, the emission light (>550 nm) was separated by a dichroic beam-splitter (570 nm), filtered (560 and 620 nm, respectively) and then detected separately by photomultipliers. The ratio of the fluorescence intensities (R560/R620; fluorescence at 560 nm relative to that at 620 nm) was calculated and converted into membrane potential. The sarcomere striations of the myocytes can be simultaneously measured by bright illumination above 650 nm (Fig. 1B). Fig. 1C shows sarcomere shortening and di-8-ANEPPS fluorescence signals at 620 and 560 nm. Although motion artifacts were apparent in the 620- and 560-nm traces, the ratiometry (R560/R620) successfully cleared the artifact (Nishimura et al., 2006a).

2.3. Membrane potential response to cardiomyocyte stretching

When transient stretches were applied to quiescent rat ventricular myocytes, transient depolarization of the membrane potential was observed. Fig. 2 shows the membrane potentials (R560/R620) together with the applied stretches quantified by the relative change in the sarcomere length (Nishimura et al., 2006a). The amplitude of the depolarization increased as the stretch magnitude was increased (Fig. 2A). When the stretch ratio exceeded 15%, action potentials were invoked in some myocytes (Fig. 2A). Administration of 10 μM gadolinium, a non-specific SAC blocker, almost completely suppressed these responses (Fig. 2B). These observations were in agreement with the predictions from computational models in which SAC activity is incorporated (Kohl et al., 1998; Rice et al., 1998; Riemer et al., 1998).

Thus, our methodology combining carbon-fiber technique with fluorescent voltage measurement enables the recording of acute changes in membrane potentials in cardiomyocytes during dynamic axial stretching. Compared with our technique, other reported techniques combining membrane potential or current measurement with axial stretching allow static or relatively slow stretches (Kamkin et al., 2000; Riemer and Tung, 2003; Zeng et al., 2000). The data presented with our current technique demonstrate that the membrane potential responds to stretch in a length-dependent manner, which was most likely dependent on SAC activation.

3. Myocardial tissue study

The impact of the mechanical stretch on cardiac electrical activity has been also studied at the ventricular level by applying balloon dilatations to the left ventricles (Franz et al., 1989, 1992; Hansen et al., 1991; Hansen et al., 1990; Lerman et al., 1985; Parker et al., 2004, 2001; Zabel et al., 1996). These studies have clarified the influence of volume pulse intensity, timing, and speed on monophasic action potentials. However, it is difficult to assess the link between volume/pressure loading stresses and the stretch levels of individual cardiomyocytes because of the complex structure of the intact ventricles. In this respect, the use of excised ventricular myocardial tissue specimens is suitable for comparisons between a global stretch (corresponding to ventricular volume pulse) with local strain (corresponding to cardiomyocyte stretch), thereby facilitating the understanding of the link between them. In this section, we introduce our studies with ventricular myocardial tissue in which we performed dynamic stretching and measured electrical activity with the optical mapping technique.

3.1. Stretching device for ventricular myocardial tissue

The use of rectangular myocardial specimens has a number of advantages for studying MEC and related arrhythmias. For example, this shape enables us to visualize two-dimensional myocardial electrophysiological activity to establish the basis of arrhythmias. Furthermore, the local strain pattern in the surface can be related to a global stretch applied to the specimen. Indeed, a number of studies of MEC have been conducted with cell cultured myocardial sheets (Kong et al., 2005; Thompson et al., 2011; Zhang et al., 2008), which provides an *in vitro* preparation that can be examined under controlled conditions. However, these models rule out the role of heterogeneous structure of the real ventricular wall, which is believed to be critical for establishing a link between the cellular MEC and arrhythmias observed at the organ level. Another disadvantage of cell culture models is that when cells are grown on a rigid surface, they cannot be stretched.

In this respect, we chose to use rectangular myocardial tissue prepared from the right ventricular (RV) free wall, thus preserving its heterogeneous structure, to assess local strain (Fig. 3A) (Seo et al., 2010). To avoid tissue ischemia, the coronary artery perfusing the RV free wall was kept intact and the aorta was connected to the Langendorff apparatus for retrograde perfusion. Cyanoacrylate tissue adhesive (Vetbond™; 3M, St. Paul, MN, USA), which is often used for sealing surgical incisions of animals, was used to glue the tissue-to-tissue supports. For our purpose, we apply a transient stretch within 200 ms. Accordingly, we chose a vibration shaker (ET-126A; Labworks Inc., Costa Mesa, CA, USA), designed for general purpose vibration testing, for applying stretch. This shaker provides a large displacement capability and high acceleration with little or no velocity restrictions, and is able to move against large loads. This shaker is equipped with a displacement transducer (IW12; TWK-Elektronik, Düsseldorf, Germany) to measure the actual displacement in response to the stretches for feed-back controls. Zirconia beads (diameter, 0.5 mm) were attached to the myocardial surface (Fig. 3A) as landmarks for motion tracking, which are used for both strain measurement and optical mapping.

3.2. Optical voltage/strain mapping in myocardial tissue

Optical mapping allows the simultaneous measurement of action potentials from a large number of recording sites with a higher spatiotemporal resolution than electrical mapping with multi-electrode arrays (Sahakian et al., 2001; Schuessler et al., 1993), and

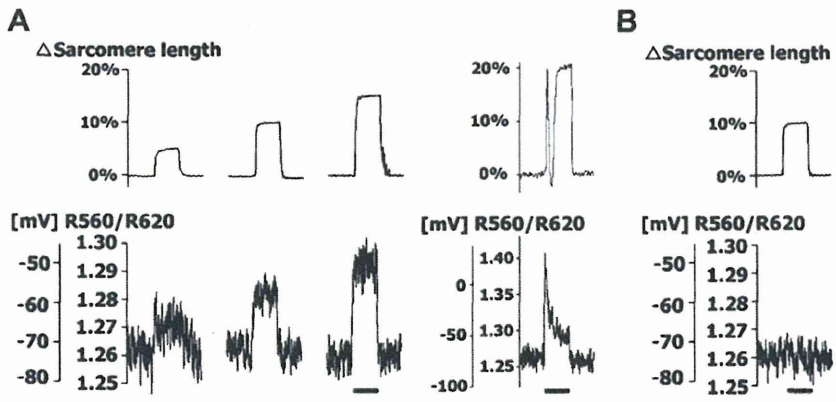

Fig. 2. Effect of dynamic stretching on resting membrane potential. A) Stretches of varying amplitudes (5%, 10%, 15%, and 20% in sarcomere length; upper traces) and the corresponding membrane potential responses (R560/R620; lower traces). Bar 500 ms. B) Effect of gadolinium (10 μM) on the resting membrane potential responses induced by dynamic stretching. Scale bar: 500 ms. The spike and notch in the sarcomere length for the 20% stretch was due to the momentary loss of length control caused by cell contraction.

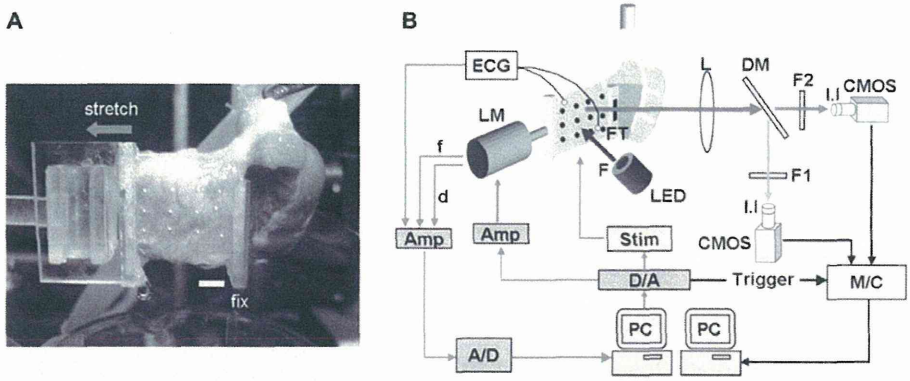

Fig. 3. Tissue preparation and the experimental setup. A) Photograph of the tissue preparation. Scale bar: 5 mm. B) Diagram of the experimental setup for tissue study. The trimmed RV wall was glued to a pair of tissue supports connected to a force transducer (FT) and a linear motor (LM). ECG, force (f) and displacement (d) signals are amplified (Amp) and recorded by a personal computer (PC) through an AD converter (A/D). Stretch and electrical stimulation commands are generated by the PC and transferred to LM and an electrical stimulator (Stim) through a DA converter (D/A). For optical voltage mapping, the tissue is illuminated by light emission diodes (LEDs). The emission light is split by a dichroic mirror (DM) and narrowed down to two frequency bands by appropriate filters (F1: 540 ± 20 nm and F2: 680 ± 20 nm). The optical images are captured by two independent CMOS cameras coupled with image intensifiers (I.I) and stored in a memory controller (M/C) and the PC. L: lens.

can be used to generate maps of electrical propagation. There also exist a number of modalities for evaluation of local strain distributions, including sonomicrometry (Toyoda et al., 2004; Villarreal et al., 1988) and tagged MRI (Moore et al., 2000; Prinzen et al., 1999). However, despite the close interdependence between electrophysiological activity and strain (i.e., MEC), there are few studies that combine multisite electrical recordings with simultaneous mechanical measurement.

We employed a marker-tracking scheme together with optical mapping to establish the relationship between strain distributions and electrical activity in cardiac preparations (Seo et al., 2010). The diagram of the experimental system is shown in Fig. 3B. The tissues were loaded with a voltage-sensitive dye, di-4-ANEPPS. Di-4-ANEPPS is known to respond to changes in the membrane potential fairly quickly and sensitively (Fluhler et al., 1985; Knisley et al., 2000), while di-8-ANEPPS, which we used in the cardiomyocyte study, has improved photostability and less phototoxicity (Bullen and Saggau, 1999; Schaffer et al., 1994). The epicardial surface of the tissues was illuminated by filtered excitation light (480 ± 10 nm) obtained from bluish-green light-emitting diodes (Nichia Chemical Industries, Tokushima, Japan), and the emitted fluorescent light was collected by a high numerical aperture complex photographic lens (50 mm F/1.2; Nikon, Tokyo, Japan), which was split by a dichroic mirror (580 nm; Andover, Salem, NH, USA) and narrowed down to two frequency bands (540 ± 20 nm and 680 ± 20 nm) through bandpass filters (Andover, Salem, NH, USA). We used two independent complementary metal oxide semiconductor (CMOS) cameras with image intensifiers (FASTCAM-Ultima; Photron, Tokyo, Japan) to simultaneously collect the dual-wavelength lights at high frame rate (500 frames/s). Conventional CMOS sensors offer advantages by achieving a very fast frame rate with a large field of view, but smaller dynamic ranges, compared with electron multiplying charge-coupled devices (EM-CCDs). On the other hand, the recent advance of scientific CMOS (sCMOS) sensors offers wide dynamic range and extremely low noise, possibly becoming major instruments for optical mapping studies (Efimov and Salama, 2012).

The optical images captured by this system have black dots arranged in a square lattice reflecting the zirconia beads attached to the tissue surface. These positional data were used for calculating epicardial local strain by dividing the distances between the bead markers in the stretched state by the corresponding distances in the reference state. This enables us to obtain local strain maps of the stretched tissue with corresponding optical maps. As noted, these positional data are also used for the motion tracking technique to remove motion-induced contamination from the optical maps.

3.3. *Image processing to remove motion artifact*

Motion artifact becomes more serious in tissue preparations, which disturbs the fluorescent signal along the light path and in the *x-y* plane. To avoid this issue, most optical mapping studies have only dealt with immobile preparations where the motion was inhibited mechanically and/or pharmacologically (e.g., butanedione monoxime and blebbistatin) (Herron et al., 2012; Lou et al., 2012). However, such preparations are nonphysiological as they ignore the role of MEC. One alternative methodological solution is to use an optical recording system based on a fiber optic image conduit, which permits the elimination of motion artifacts in myocardial tissue (Rohr and Kucera, 1998), although the number of the recording site is limited. By contrast, we have used ratiometry combined with a motion-tracking technique to resolve the problem in optical mapping (Inagaki et al., 2004; Seo et al., 2010). For motion tracking, the initial images were used as a reference, and the corresponding positions of the bead landmarks attached to the tissue surface in the successive image were automatically determined by template matching of the image of each bead. We used the positional data to determine the affine transformation matrices for the geometric distortion during the stretch or contraction. With the affine transformation based on motion tracking, we traced the tissue points, presumably a cluster of specific myocytes, during a stretch, and showed the sequential changes in the transmembrane potential of each tissue segment. Throughout the course of calculations, ratiometry with numerator wavelengths of 540 ± 20 nm and denominator wavelengths of 680 ± 20 nm was used to remove the artifacts caused by motion along the light path.

To compensate for motion artifact, other researchers have also used affine transformation (Rohde et al., 2005; Svrcek et al., 2009) or non-linear transformation (Westergaard et al., 2008). Another reported method involves the use of grid points surrounded by a constant control area in each frame to find best matches with those of the reference frame (Bagwe et al., 2005). The major difference between these techniques and ours is the use of landmarks for motion tracking, which enables more stable tracking. In fact, the images without landmarks are often devoid of distinct features, which makes it difficult to track the motion especially in the dynamically stretched tissue. The use of landmarks also facilitates

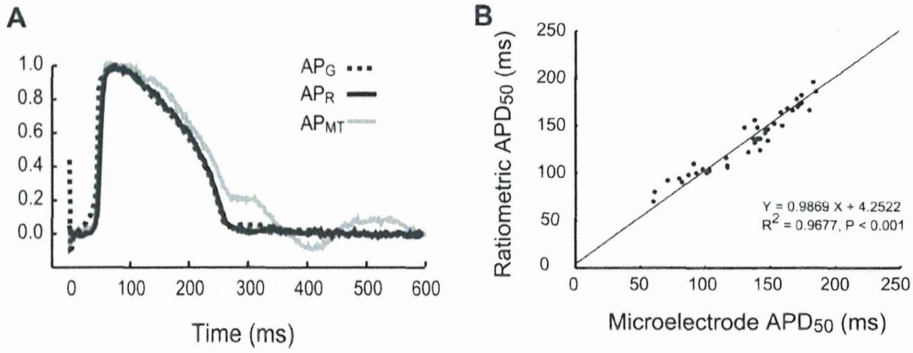

Fig. 4. Optical membrane potentials after motion tracking and/or ratiometric processing. A) Intracellular glass microelectrode signal (AP_G), ratiometric signal (AP_R), and 540 ± 20 nm wavelength signal after motion tracking (AP_{MT}). B) Scatter plot of action potential duration at 50% repolarization (APD_{50}) obtained from ratiometric and simultaneous microelectrode recordings ($n = 7$).

the quantification of epicardial strain distribution. Bourgeois and colleagues recently developed a similar but sophisticated technique in which ring-shaped markers were used for motion tracking to successfully remove motion artifact generated by heart contraction (Bourgeois et al., 2011).

Fig. 4A shows typical action potential recordings (540 ± 20 nm wavelength signal after motion tracking processing, and the ratiometric signal) from the optical mapping system, and a simultaneous recording from an intracellular glass microelectrode in the freely beating rabbit ventricle (Inagaki et al., 2004). In both optical signals after the motion tracking, the action potentials upstroke is not contaminated by motion. However, in the 540 ± 20 nm wavelength signal, the action potential plateau and repolarization remain distorted by the motion artifact. We found that ratiometry removed this artifact and gave a similar action potential contour to that obtained from a microelectrode signal. The combined results shown in Fig. 4B indicate agreement of action potential duration at 50% repolarization measured ratiometrically with that measured from microelectrode signals.

3.4. Stretch-induced excitation in myocardial tissue

The use of this technique in a tissue preparation provided us with a unique opportunity to elucidate the relationships among

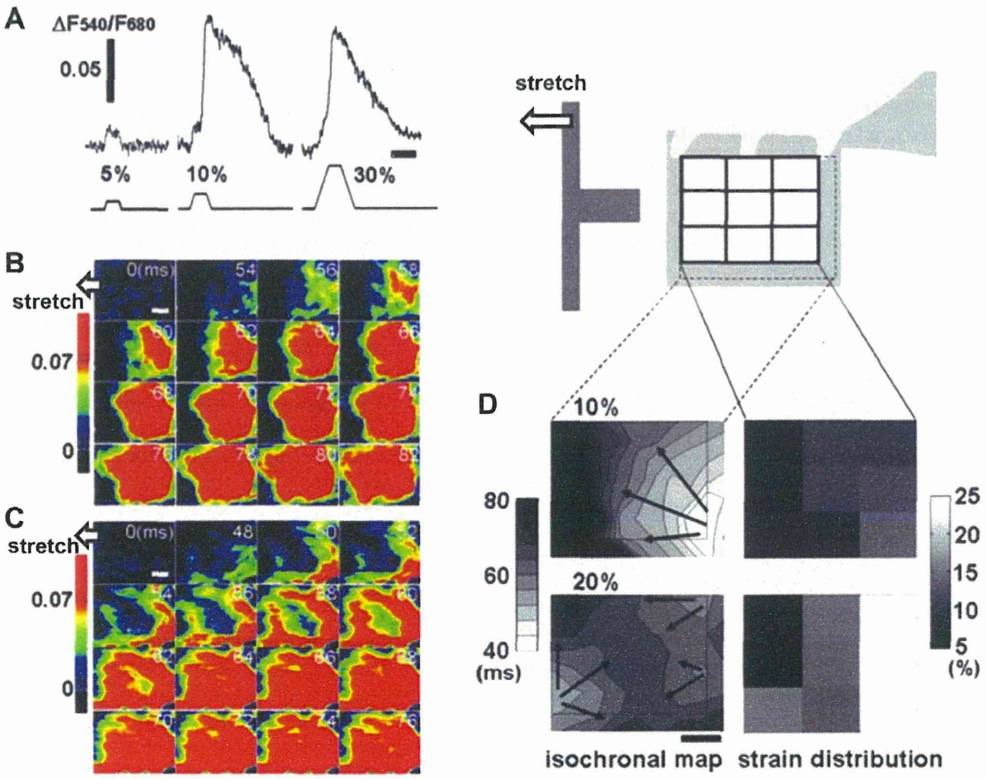

Fig. 5. Alterations in the electrical activation and strain distributions in cardiac tissues in response to stretches. A) Ratiometric optical signals in response to 5%, 10%, and 30% stretches. Scale bar: 100 ms. B and C) Representative optical maps in response to 10% and 30% stretches, respectively. The left side of the tissue was stretched leftward. The stretch starts at 0 ms. Scale bar: 4 mm. D) Representative isochronal maps of transmembrane potentials (left) and strain distributions (right). Top and bottom show 10% and 20% stretch, respectively. Scale bar: 4 mm.

electrical excitation, global strain, and local strain. Fig. 5A shows representative transmembrane potential signals in response to stretches of varying amplitudes (Seo et al., 2010). With a uniaxial stretch with a small amplitude (5%), the myocardial tissue was depolarized but an action potential was not invoked (Fig. 5A left). Above a certain level of amplitude (≥10%), however, focal excitation and its propagation were observed (Fig. 5A middle, Fig. 5B). A larger stretch (30%) induced multiple excitations (Fig. 5A right, Fig. 5C). Evaluation of the relevance between stretch-activated excitation and epicardial local strain revealed that although a uniaxial global stretch was applied to the preparation, excitation was usually only induced in a limited area where the local strain was high (Fig. 5D). Furthermore, this heterogeneity in the strain distribution reflected the complex structure of the ventricular wall, such that the excitation is initiated in regions where the wall is thin (Seo et al., 2010). This finding is supported by other experimental evidence showing that an increase in intraventricular volume by pulmonary arterial occlusion results in non-uniform stretch of the right ventricular wall, which is associated with different alterations in regional monophasic action potential morphology, including the initiation of early after depolarizations (Chen et al., 2004). Accordingly, with increased intraventricular stress, excitations are usually initiated from the region of largest strain (Quinn, 2014). Whereas the heterogeneous structure of the ventricles normally works for its vigorous contraction, adverse hemodynamic overloads in disease states lead to abnormalities in the ventricular shape and regional wall motion (Katz and Katz, 1989), which may sometimes evoke focal excitations from thinner areas.

4. Relevance of cellular mechano-electric coupling to stretch-induced arrhythmias

The mechanisms by which mechanical stretches can lead to fatal arrhythmias have been predominantly investigated by computer simulation (Pfeiffer et al., 2014; Quinn, 2014; Quinn and Kohl, 2011; Trayanova et al., 2011). Two-dimensional (Garny and Kohl, 2004) and three-dimensional (Li et al., 2004) models of ventricular tissue have demonstrated that mechanically induced sustained arrhythmias (i.e., re-entry) may occur only when focal excitations initiated by mechanical stimuli interact with the preceding electrical activation of the myocardial tissue. Our experimental results suggest that the focal excitation can be induced with intermediate-strength mechanical stimuli. To elucidate the link between the focal ectopic excitation and a fatal arrhythmia, detailed evaluation of spatio-temporal electrical behavior is necessary. Therefore, we investigated the characteristics of mechanically-induced ectopy in the whole heart and its potential for inducing sustained fatal arrhythmias with our modified optical mapping system (Fig. 6A) coupled with the motion tracking and the image processing techniques introduced in the tissue study. We applied a controlled volume pulse to the isolated Langendorff-perfused rabbit RV at various coupling intervals (90–130 ms) with a preceding electrical stimulus (Seo et al., 2010). As shown in Fig. 6B, we observed re-entrant arrhythmias with a volume pulse of intermediate size (1.5 mL). As shown in Fig. 6C, a large volume pulse (2 mL) did not elicit arrhythmias. Importantly, only an intermediate volume pulse (1.5 mL) applied after a proper coupling interval (110 ms) triggered re-entrant arrhythmias.

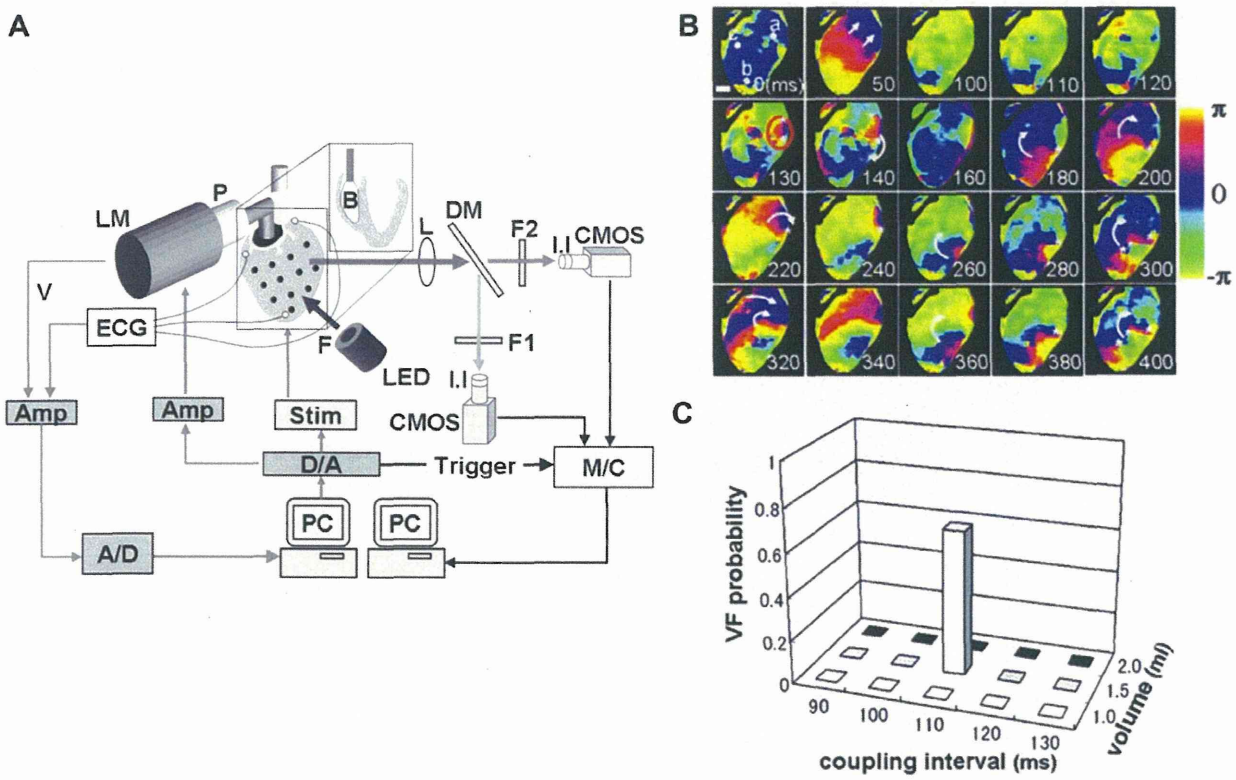

Fig. 6. Occurrence of stretch-induced re-entrant arrhythmias in the whole heart preparations. A) Diagram of the experimental setup for whole heart study. This system is a modified version of the tissue stretching system described in Fig. 3B. A balloon (B) is inserted into RV of the perfused whole heart and is connected to a piston pump (P) with a linear motor (LM) to apply servo-controlled volume pulses. B) Representative phase maps of re-entrant arrhythmia. The volume pulse (1.5 mL) was applied at 110 ms after an electrical stimulus started at 0 ms. Scale bar: 4 mm *Phase singularity points. C) Excitation probabilities in relation to the coupling intervals and the intensities of the volume pulses ($n = 3$).

There are extensive studies examining the electrophysiological effects of volume increases in the intact heart (Franz et al., 1989, 1992; Hansen et al., 1991; Hansen et al., 1990; Parker et al., 2004, 2001; Zabel et al., 1996). For example, Hansen et al. examined the effects of rapid, transient, volume increases in an isolated, perfused, canine ventricle, and observed ectopic excitations during or shortly after the volume pulse, although they did not record direct electrophysiological behavior (Hansen et al., 1990). Franz et al. also investigated the effects of increases in ventricular diastolic volume on epicardial monophasic action potentials in Langendorff perfused rabbit hearts, and clearly demonstrated its effect on the incidence of extrasystole (Franz et al., 1992). However, no experimental studies have succeeded in determining the characteristics of stretch-induced fatal arrhythmias with this preparation. Recent advances in optical mapping and its combination with our motion-tracking technique provide the first evidence that the re-entrant arrhythmias can be induced by intermediate-volume pulse coupled with preceding electrical stimulation (Fig. 6B) (Seo et al., 2010). One of the limitations in our system is that the mapped region in the intact heart is restricted to the field of view of the sensor, which makes it difficult to track electrical waves as they can drift in and out of view. To overcome this problem, novel techniques to image the entire surface (front and back) of the heart such as panoramic imaging are needed (Bourgeois et al., 2012; Kay et al., 2006).

Our proposed mechanism of how cellular MEC leads to fatal arrhythmias observed in the whole heart preparation is shown in Fig. 7. First, membrane potential responds to stretch in an amplitude-dependent manner in single cardiomyocytes (Fig. 2). At the tissue level, conversely, the electrical activity is highly heterogeneous especially when the intermediate strength of global stretch is applied to the tissue (Fig. 5). This is because of the modulation by the inhomogeneous structure of the ventricular wall. At the organ level, when the medium volume pulse is applied at a certain coupling interval, the stretch-induced focal excitation can develop into fatal re-entrant arrhythmias (Fig. 6). This scenario may explain the etiology of *commotio cordis*, which often occurs because of a nonpenetrating chest wall blow when the rib, sternum, and heart are themselves uninjured. Indeed, experimentally, *commotio cordis* was reported to be induced by baseball projectiles with intermediate strength (Link et al., 2003), although the mechanisms have been elusive. Our studies indicate the non-uniformity of the ventricular wall structure is associated with a high susceptibility to fatal arrhythmias, which may be a predictor of sudden cardiac death.

5. Future directions: laser optical trap combined with real-time Ca^{2+} imaging in cardiomyocytes

In this review, we have described our observations of mechanical stress-induced electrical activities made at cell, tissue, and organ levels, and discussed their inter-relationships. However, to gain further insight into the mechanisms underlying mechanical stress-induced electrical activity, we need to extend our limit of observation to the subcellular level. As the first step toward this goal, we made a preliminary attempt to determine how cardiomyocytes respond to a minute stimulus applied to the sarcolemma. As an actuator to apply a stimulus of small magnitude, we adopted the laser optical trap technique (Sugiura et al., 1998) with which we can trap and manipulate a small bead under a microscope (IX70; Olympus, Tokyo, Japan) using an infrared laser beam (1064 nm IRCL-1W; CrystaLaser, Reno, NV, USA) introduced via an objective lens (60×, n.a. 1.4). Cardiomyocytes isolated from 6-week-old Wistar rats were loaded with calcium indicator (Fluo-8) and fixed on laminin-coated coverslips in buffer containing 1.1 mM Ca^{2+}. To this preparation we added a small bead (diameter 6.0 μm Polybead Carboxylated; Polysciences Inc., Warrington, PA, USA) coated with an RGD peptide (Sigma–Aldrich, St. Louis MO, USA) as the selective ligand to integrin. We selected a bead firmly attached to the sarcolemma, and then trapped and moved it with the optical trap

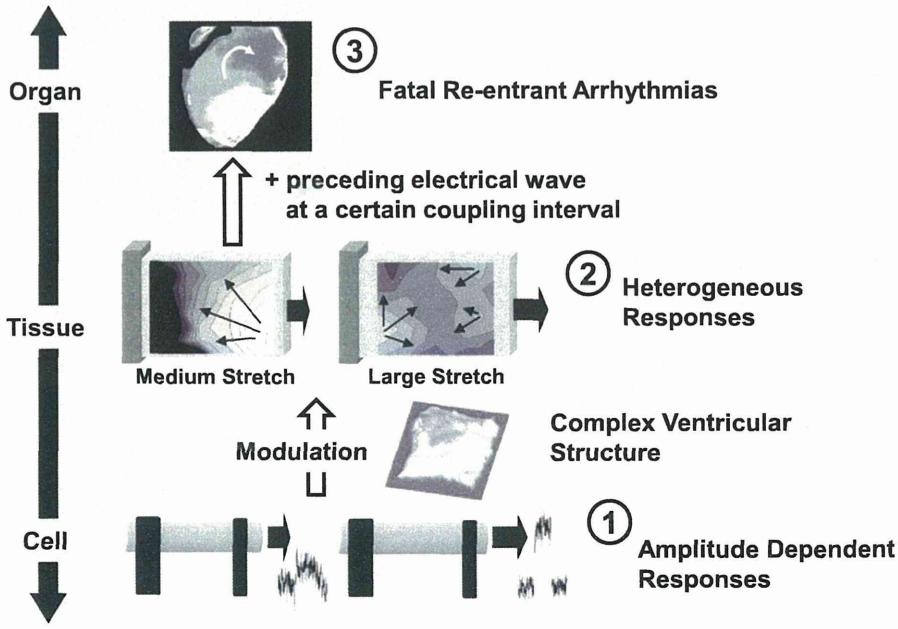

Fig. 7. Schematic illustration of our proposed mechanism. (1) At the cellular level, membrane potential responds to stretch in an amplitude-dependent manner. (2) At the tissue level, however, globally applied stretch is modulated by the inhomogeneous structure of the ventricular wall to cause heterogeneous excitation. (3) This effect becomes manifest in response to stretch of medium intensity and may trigger fatal arrhythmias when coupled with a preceding electrical propagation.

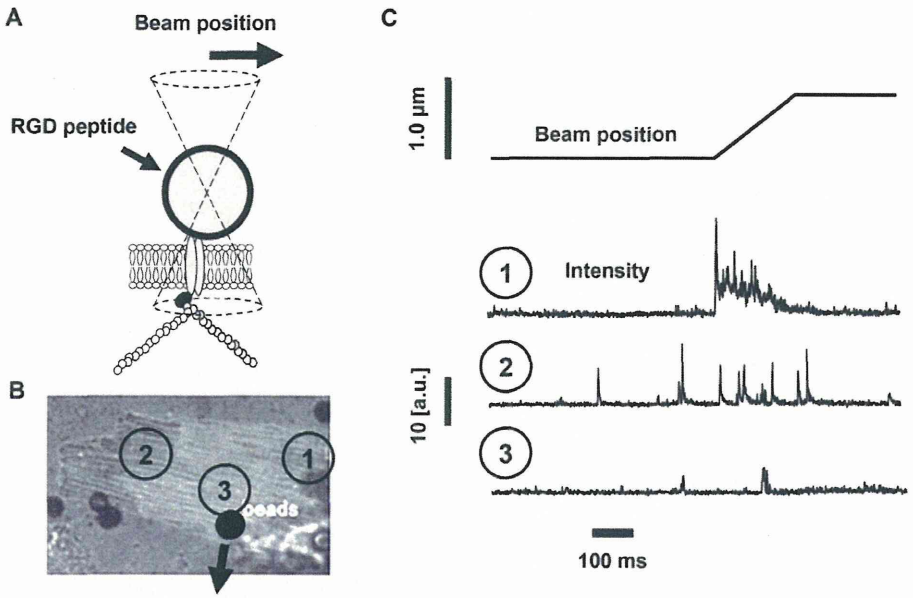

Fig. 8. Ca^{2+} spark responses to subcellular level stimulus. A) A microsphere coated with RGD peptide was attached to the sarcolemma and trapped by the laser optical trap. Stimulus of small amplitude was applied by moving the laser beam. B) The microsphere was moved in the transverse direction (arrow) and the fluorescent signals were sampled at three locations in the same cell. C) Top row: displacement of the laser beam. 2nd to 4th rows: fluorescent signals from the Ca^{2+} indicator at 3 locations indicated in B. Ca^{2+} sparks coincided with the mechanical stimulus were observed in the locations remote from the stimulus site (1 and 2).

linearly with a small amplitude (<1 μm) by steering the galvanomirror equipped in the beam path (Fig. 8A). Fluorescent images were viewed and recorded by spinning disc confocal laser scanning microscope (CSU-X1; Yokogawa, Tokyo, Japan) with a high-speed camera (SV-200i; Photoron, Tokyo, Japan). The detailed method is described in the online supplementary material.

The applied stimulus provoked calcium sparks, but they were clustered in a remote area rather than at the site of the stimulus (Fig. 8B and C). Furthermore, treatment with colchicine, which inhibits microtubule polymerization, abolished these responses (data not shown). Although the number of observations is limited, these data suggest a role of the cytoskeletal network in the transmission of a mechanical stimulus within the myocyte, consistent with earlier reports (Iribe et al., 2009; Prosser et al., 2011). This may be related to the observation by Parker that treatment with taxol, which polymerizes microtubules, increased the frequency of arrhythmias induced by volume pulse to the rabbit left ventricles (Parker et al., 2001). By contrast, in a swine model of *commotio cordis*, colchicine treatment increased the probability of chest impact-induced ventricular fibrillation (Madias et al., 2008).

It has been demonstrated that Ca^{2+} waves can be initiated in damaged myocardial region where non-uniform muscle are subjected to contraction-associated stretch, which may lead to premature beats and triggered arrhythmias (ter Keurs, 2012; Wakayama et al., 2005). Such a non-uniform activity in myocardium is often observed in pathological state such as myocardial infarction and heart failure (Quinn, 2014). It is evident that acute stretch of ventricles can result in re-entrant arrhythmias by triggering through stretch-induced changes in membrane potential (Seo et al., 2010), although intracellular Ca^{2+} handling may play other roles especially in diseases. Although further studies are needed, continuing studies at multiple biological system levels and possible integration by numerical simulation will help further our understanding of mechanical stress-induced arrhythmia and to develop effective preventative measures.

6. Conclusions

In this review, we introduced our unique experimental techniques in various experimental settings. Our studies provide a possible scenario for the link between cardiomyocyte MEC and fatal arrhythmias induced by acute mechanical stresses. Further development and utility of these techniques will promote basic studies and a comprehensive understanding of the molecular mechanisms of MEC and its translation to stretch-induced arrhythmias.

Editors' note

Please see also related communications in this issue by Yu et al. (2014) and Wang et al. (2014).

Acknowledgments

This research is supported by the Japan Society for the Promotion of Science (JSPS) through its "Funding Program for World-Leading Innovative R&D on Science and Technology (FIRST Program)" and the JSPS Postdoctoral Fellowship for Research Abroad to K. S.. Figs. 1 and 2 were reprinted from Cardiovascular Research 72, Nishimura, S., Kawai, Y., Nakajima, T., Hosoya, Y., Fujita, H., Katoh, M., Yamashita, H., Nagai, R., Sugiura, S., Membrane potential of rat ventricular myocytes responds to axial stretch in phase, amplitude and speed-dependent manners, pp. 403–411, 2006, with permission from Oxford University Press. Figs. 3, 5 and 6 were reprinted from Circulation Research 106, Seo, K., Inagaki, M., Nishimura, S., Hidaka, I., Sugimachi, M., Hisada, T., Sugiura, S., Structural Heterogeneity in the Ventricular Wall Plays a Significant Role in the Initiation of Stretch-Induced Arrhythmias in Perfused Rabbit Right Ventricular Tissues and Whole Heart Preparations, pp. 176–184, 2010, with permission from Wolters Kluwer Health. Fig. 4 was reprinted from Proceedings of the 26th Annual International Conference of the IEEE EMBS, Inagaki, M., Hidaka, I., Aiba, T., Tatewaki, T., Sunagawa, K., Sugimachi, M., High resolution optical mapping of